Supplement of

Constructing nationally comprehensive annual rice paddy maps for Madagascar from 2017 to 2025

Ryoungseob Kwon[1,2], Youngryel Ryu[1,2,3,4]*, Giacomo De Nicola[5], Hervet Randriamady[5], Oladimeji Ezekiel Mudele[5], Tinashe Tapera[5], Hyeyoung Jo[1], Christopher D. Golden[5]*

[1] Interdisciplinary Program in Landscape Architecture, Seoul National University, Seoul, Republic of Korea

[2] Integrated Major in Smart City Global Convergence, Seoul National University, Seoul, Republic of Korea

[3] Department of Landscape Architecture and Rural Systems Engineering, Seoul National University, Seoul, Republic of Korea

[4] SNU Energy Initiatives, Seoul National University, Seoul, Republic of Korea

[5] Department of Nutrition, Harvard TH Chan School of Public Health, Boston, Massachusetts, United States of America

Correspondence to: Youngryel Ryu (yryu@snu.ac.kr) and Christopher D. Golden (golden@hsph.harvard.edu)

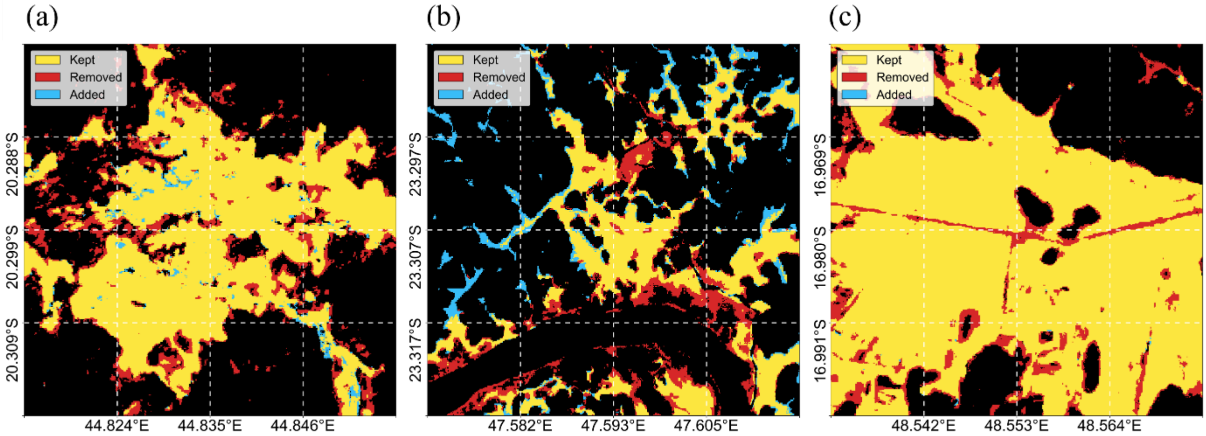

Figure S1. Pixel-level refinement from the first-stage to the second-stage rice classification at three representative sites in Madagascar. Yellow shows pixels classified as rice in both stages, red shows pixels classified as rice in the first stage but reclassified as non-rice in the second stage, and cyan shows pixels added as rice in the second stage but not in the first stage.

Table S1. Share of the mapped rice paddy area by slope class in Madagascar from 2017 to 2025. Slope was derived from the 30 m Shuttle Radar Topography Mission dataset, and values denote the percentage of the annual national rice paddy area within each slope class.

Year	**< 2°**	**2–5°**	**5–10°**	**> 10°**
2017	61.1	33.5	4.9	0.47
2018	63.9	32.1	3.7	0.29
2019	59.8	33.9	5.7	0.58
2020	62.7	32.8	4.2	0.35
2021	60.8	34.0	4.8	0.40
2022	60.6	34.0	5.0	0.42
2023	61.1	33.6	4.8	0.41
2024	63.1	32.6	4.1	0.33
2025	61.2	33.6	4.7	0.40
Mean	**61.6**	**33.4**	**4.7**	**0.41**

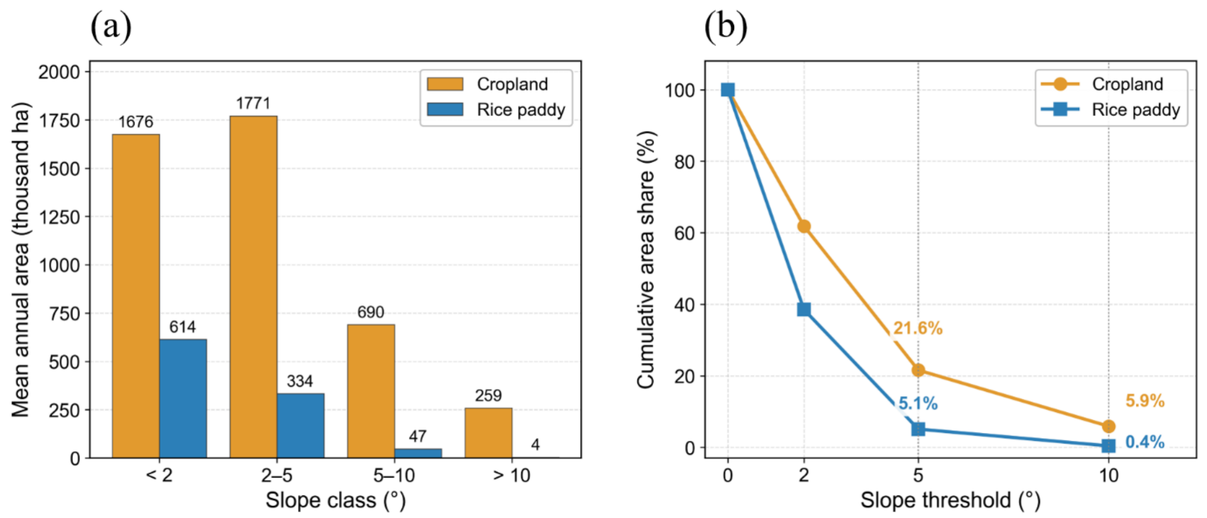

Figure S2. Distribution of rice paddy and cropland area across slope classes in Madagascar. (a) Mean annual area (2017–2025) of the mapped rice paddy and of cropland within each slope class. (b) Cumulative share of the rice paddy and cropland area on slopes steeper than a given threshold. Slope was derived from the 30 m SRTM dataset following the Horn method.

Figure S3. Zoomed-in visualizations of pseudo-labeled samples showing their spatial distribution generated using phenology-based rules for (a) rice paddy, (b) other crops, and (c) wetlands across diverse regions of Madagascar (background imagery: Imagery © 2026 CNES/Airbus, Maxar Technologies; Map data © 2026 Google).

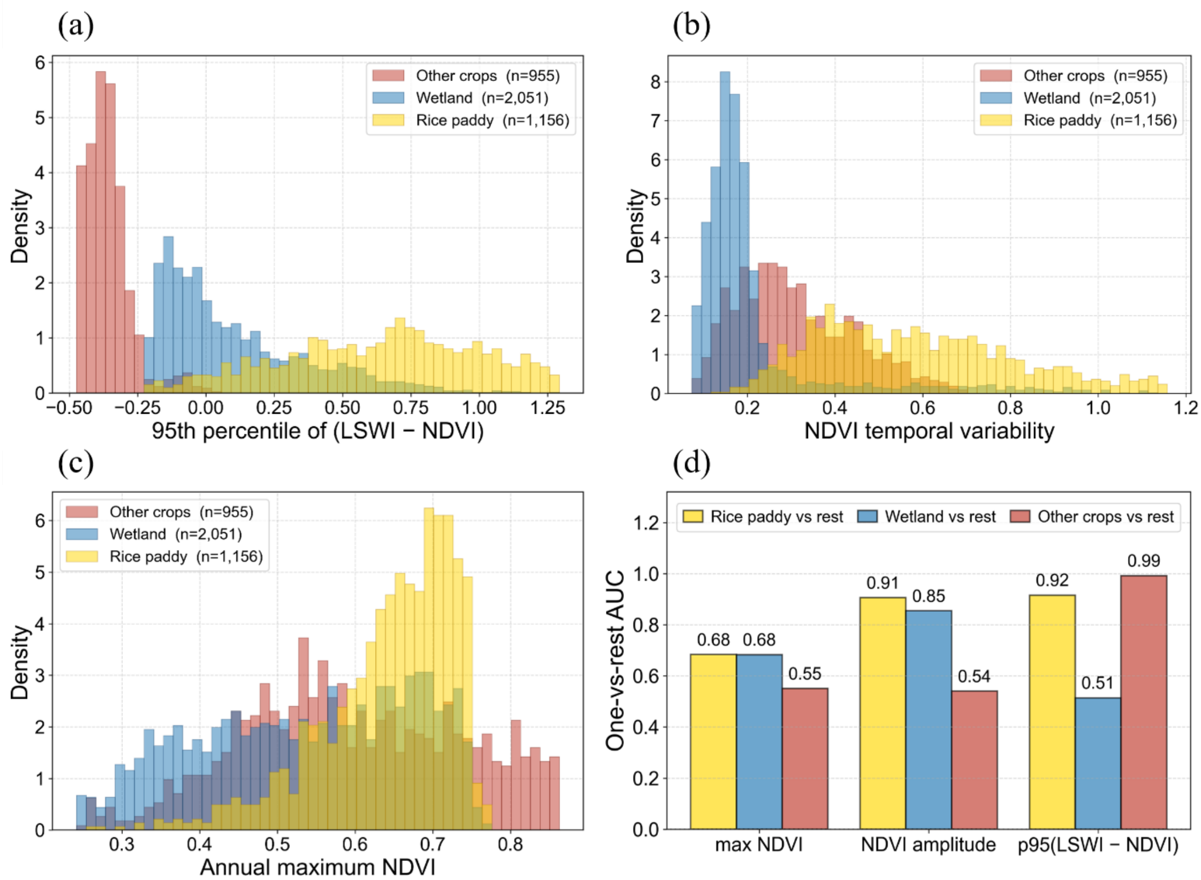

Figure S4. Phenological feature distributions and single-feature class separability for the three pseudo-label categories. Density histograms of (a) the 95th percentile of the LSWI–NDVI difference, (b) NDVI temporal variability, and (c) annual maximum NDVI for rice paddies (yellow), flooded wetlands (blue), and other crops (red). One-vs-rest AUC per feature quantifies how well a single feature separates the target class from the others.

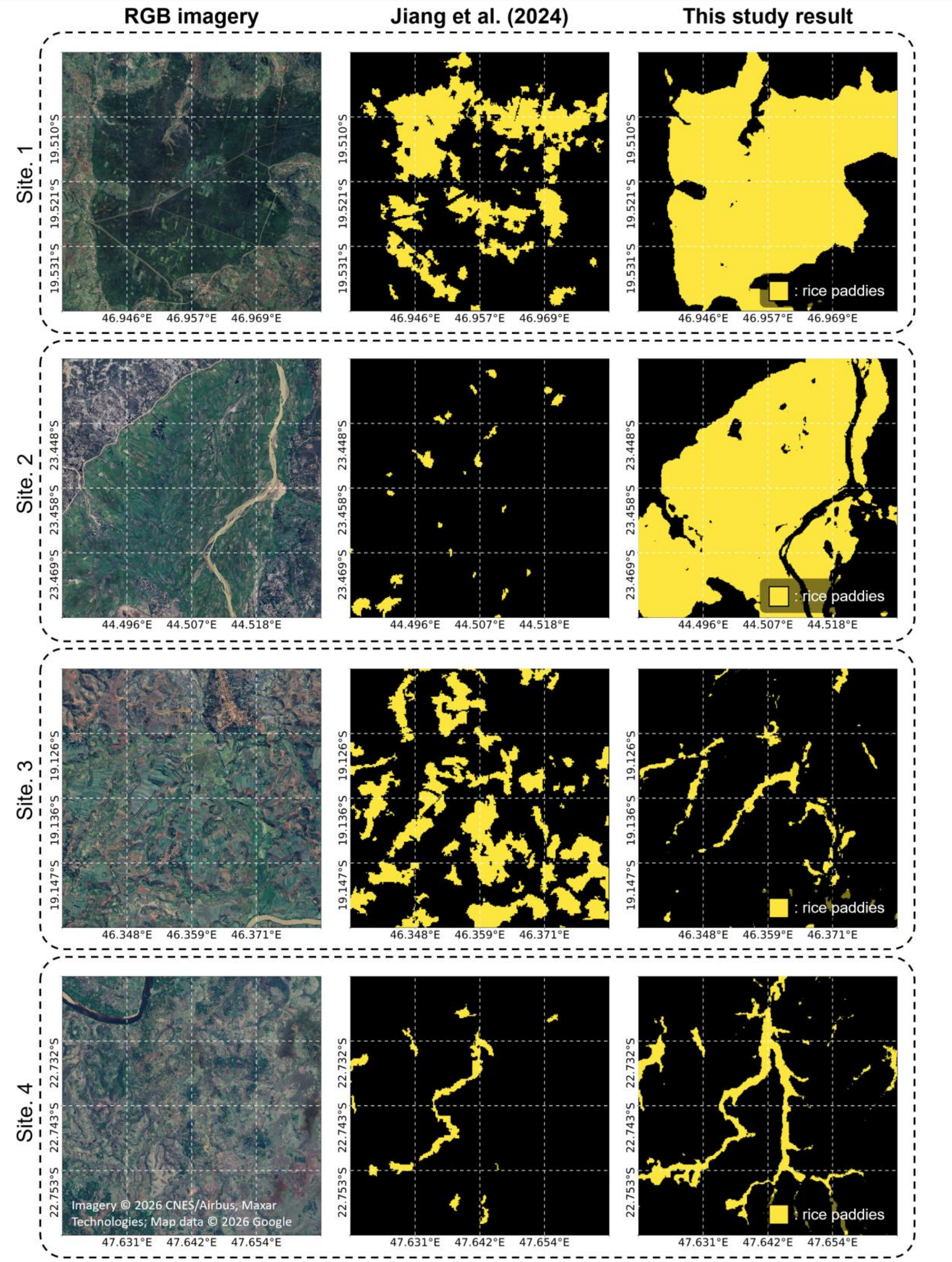

Figure S5. Visual comparison between the benchmark product and our rice paddy map at four representative sites in Madagascar. The left column shows Google Satellite RGB imagery for context, the middle and right column show rice paddy pixels (yellow) from the benchmark and this study, respectively (background imagery: Imagery © 2026 CNES/Airbus, Maxar Technologies; Map data © 2026 Google).

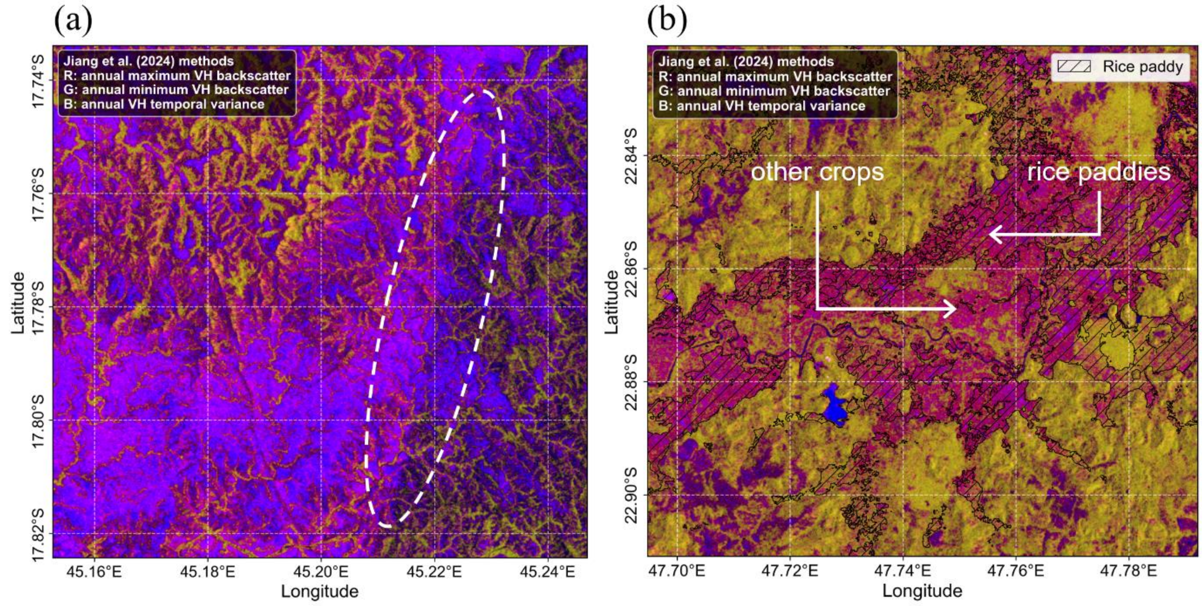

Figure S6. Two representative sites in Madagascar illustrating the limitations of the SAR-based rice pseudo-labeling method proposed by Jiang et al. (2024). Background images show Sentinel-1 VH pseudo-color composites (R: annual maximum, G: annual minimum, B: annual temporal variance of VH backscatter), and black hatched polygons indicate pixels classified as rice paddies in this study.

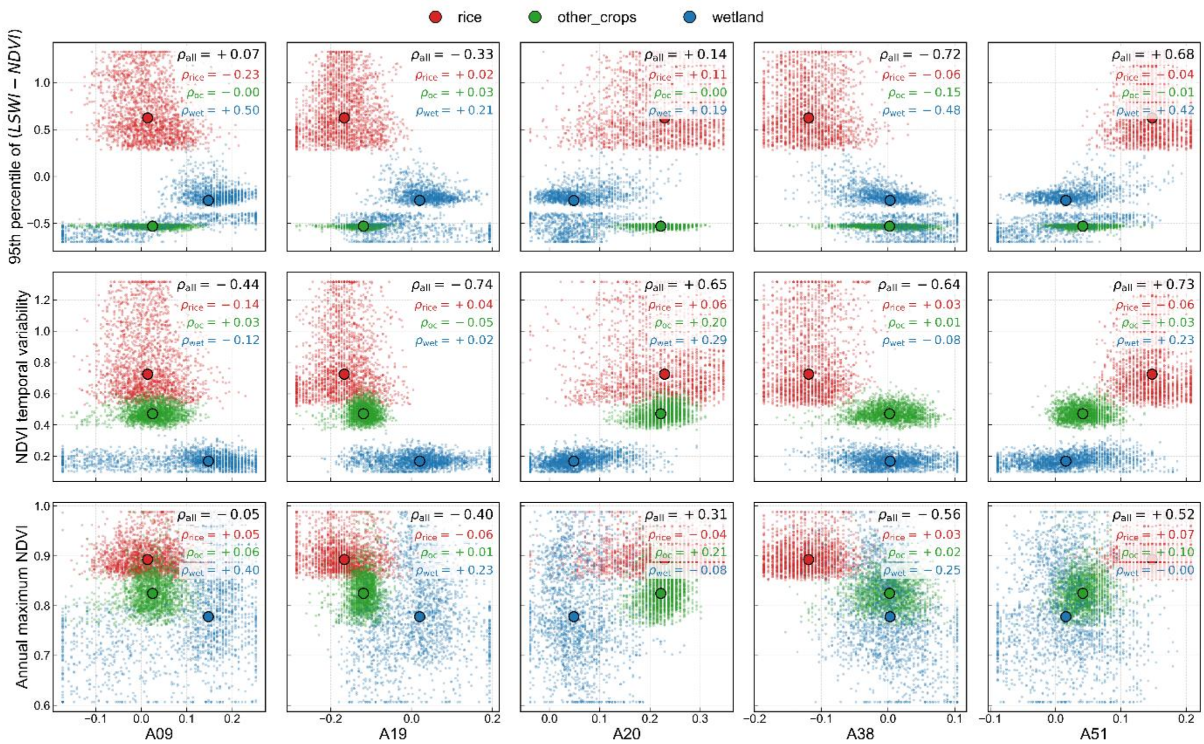

Figure S7. Relationship between the top-5 GSE dimensions (A09, A19, A20, A38, A51) and three HLS-derived phenological metrics (95th percentile of the difference between LSWI and NDVI, NDVI temporal variability, and annual maximum NDVI), evaluated at pseudo-label sample points generated across 2017-2025 (3,000 points per class per year). Filled circles with black edges mark the per-class median in each panel. Spearman rank correlation coefficients are reported in each panel.

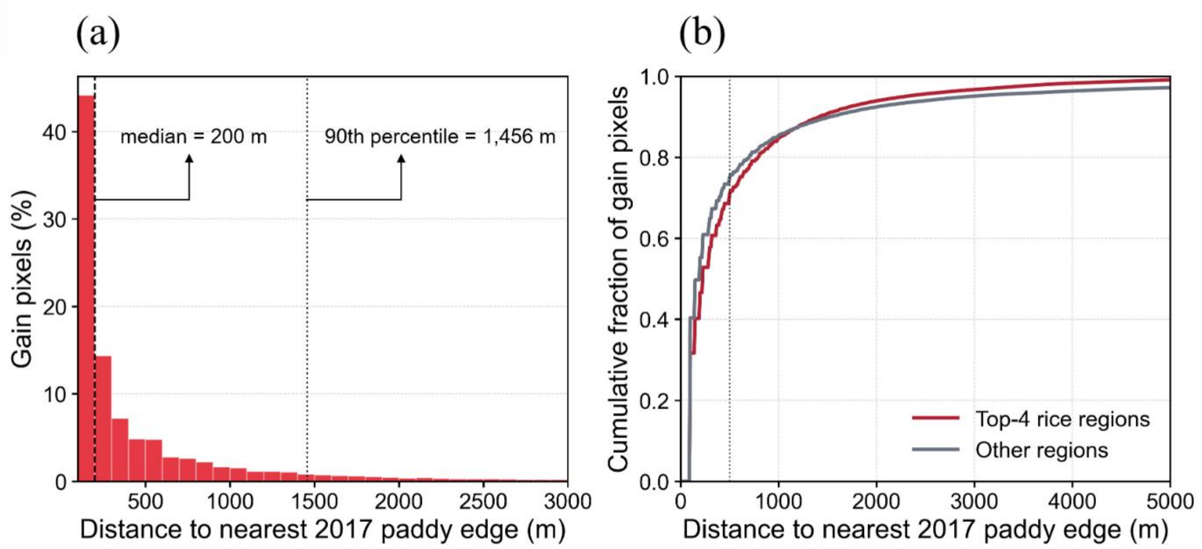

Figure S8. Distance of 2025 rice paddy gain pixels from the nearest 2017 paddy edge, including (a) histogram of distances (m) for all gain pixels, with vertical dashed and dotted lines indicating the median and the 90th percentile, and (b) cumulative distribution of distances, comparing the top-4 rice-producing regions (Boeny, Betsiboka, Alaotra-Mangoro, and Menabe) with the remaining regions.

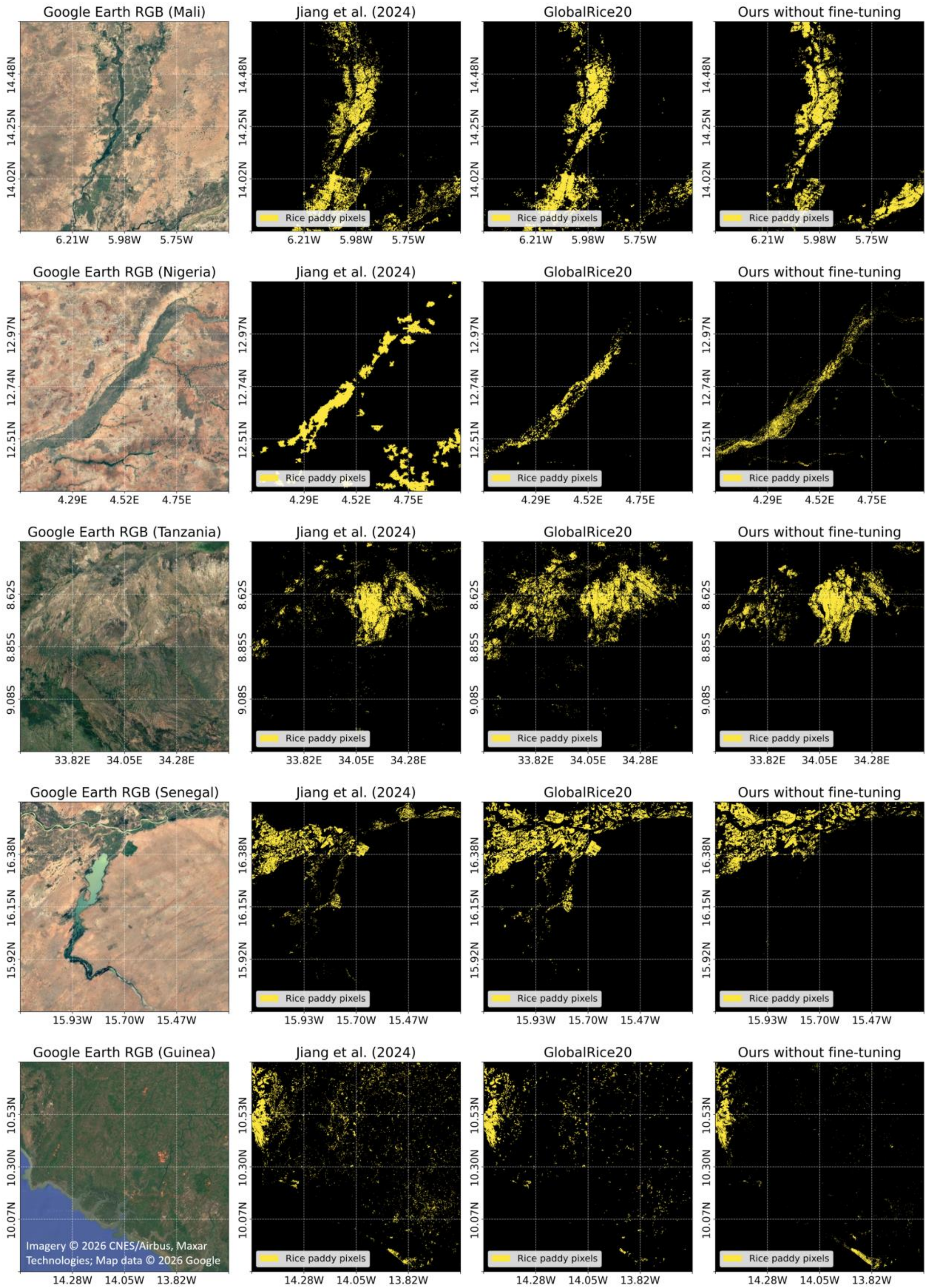

Figure S9. Exploratory spatial transferability assessment of the Madagascar-trained rice paddy mapping framework in selected African rice-producing regions. Each row shows Google Earth RGB imagery, the Jiang et al. (2024) benchmark product, GlobalRice20 (Zhang et al., 2026), and our result without country-specific fine-tuning. Yellow pixels indicate mapped rice paddies (background imagery: Imagery © 2026 CNES/Airbus, Maxar Technologies; Map data © 2026 Google).